Peng Gao, Yong-Fei Zheng, Matthew Jason Mayne, and Zi-Fu Zhao, 2020, Miocene high-temperature leucogranite magmatism in the Himalayan orogen: GSA Bulletin, https://doi.org/10.1130/B35691.1.

Supplemental Material

Supplementary Materials I: Figures S1 to S6

Figure S1. Photographs of field (A) and hank specimen (B) as well as microphotographs of the two-mica granites from Yalaxiangbo. (C) and (D) are under plane-polarized light and cross-polarized light, respectively, both from sample 15XZ390. Mineral abbreviations: Bt–biotite, Ms–muscovite, Pl–plagioclase, Kfs–K-feldspar.

Figure S2. Zircon U–Pb concordia diagrams for the Yalaxiangbo granites (the first left panels; Table S1) and CL images of representative zircons from the Yalaxiangbo granites (the three right panels). Each row comes from the same sample. The green and red circles are analytical positions of O isotope and U–Pb isotopes + trace elements, with diagrams of 20 μm and 32 μm, respectively. Scale bar is 100 μm. Analytical results of U–Pb ages, δ18O values and Ti contents are also labeled. The rightmost three images show relict zircon surrounded by dark and thin rims which cannot be analyzed. Analytical number is shown in white italic.

Figure S3. Results of condition experiments showing the influences of initial water content and oxygen fugacity on the activities (aSiO2 and aTiO2) and corrected temperatures derived from Ti-in-zircon thermometer. Sample 15XZ390 is used for modeling. Crystallization pressure is set to 4 kbar. The modeling results are listed in Tables S3 and S4.

Figure S4. (A) Results of condition experiments showing the influence of crystallization pressure on the corrected temperatures derived from Ti-in-zircon thermometer. Sample 15XZ390 is used for modeling. Initial water content and oxygen buffer are set to 4 wt% and FMQ, respectively. The modeling results are listed in Table S3. (B) Results of modeled melt fraction (wt%) versus crystallization temperature. Crystallization pressure and oxygen buffer are set to 4 kbar and FMQ, respectively. Three initial water contents (3, 4, 5 wt%) are considered. The modeling results are listed in Table S4.

Figure S5. Results of modeled melt fraction (vol%) versus melting temperature derived from six pelite samples at 6, 8, and 10 kbar. Starting materials used for modeling are given is Table S5 and the modeling results are listed in Table S6. Oxygen buffer FMQ is used. 'Melt connectivity transition' from Rosenberg and Handy (2005) at 7 vol% melt is shown for comparison.

Figure S6. Plots of zircon trace element compositions of the three Miocene Yalaxiangbo granites. Data are given in Table S1. Data for Tsona granites in panels (A) and (B) are from Aikman et al. (2012b).

Supplementary Materials II: Methodology

TABLES S1–S8

Table S1. U-Pb isotope, trace element and O isotope compositions of zircon from the Miocene Yalaxiangbo granites.

Table S2. Whole-rock major-trace element, O isotope and Sr-Nd compositions of the Miocene Yalaxiangbo granites.

Table S3. Ti contents measured in zircons from the Miocene Yalaxiangbo granites and calculated Ti-in-zircon temperatures according to Ferry and Watson (2007).

Table S4. Temperature-activity relation for sample 15XZ390 at a variety of conditions. Melt fraction at FMQ is also listed.

Table S5. Major element compositions of six pelite samples used for modeling.

Table S6. Modeled melt fraction (vol%) from six pelite samples.

Table S7. Modeled melt compositions (wt%) from three Na-rich pelites.

Table S8. Major-element compositions of major rock-forming minerals from sample 15XZ390 measured by EMPA.

Supplementary Materials I: Additional diagrams

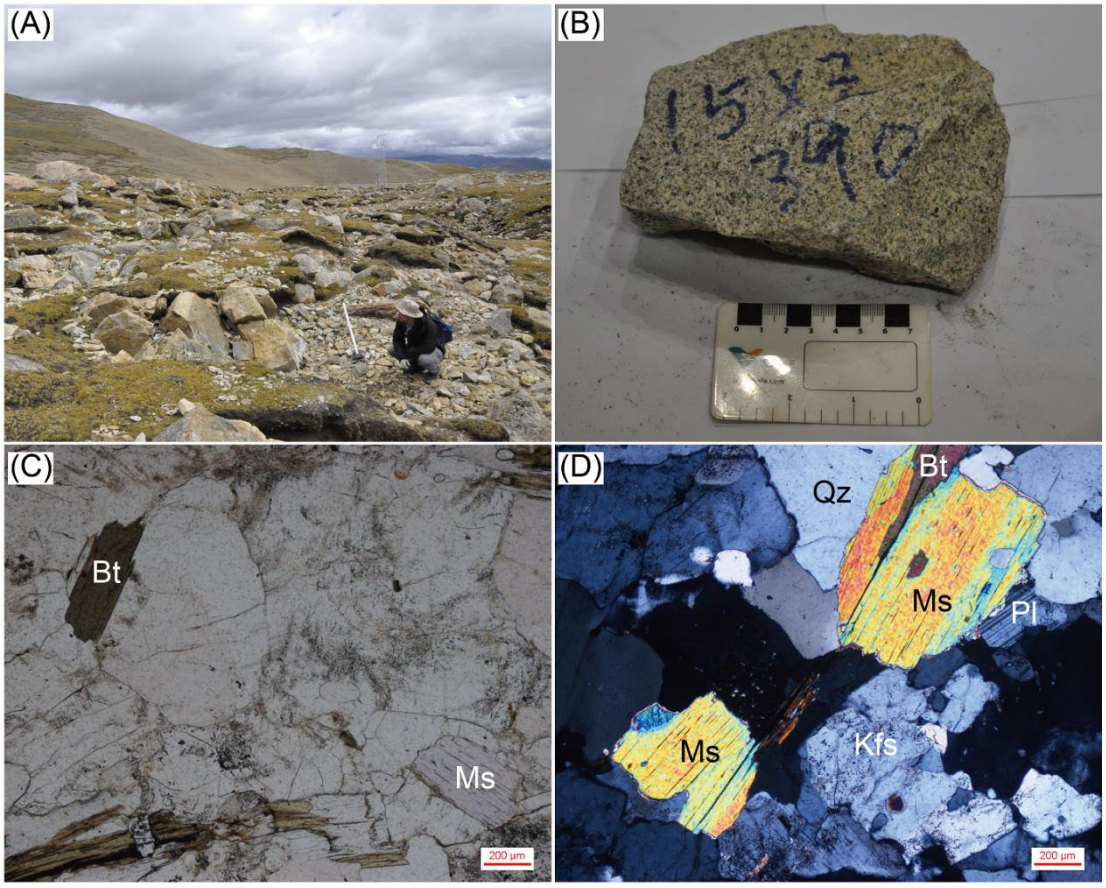

Figure S1. Photographs of field (A) and hank specimen (B) as well as microphotographs of the two-mica granites from Yalaxiangbo. (C) and (D) are under plane-polarized light and cross-polarized light, respectively, both from sample 15XZ390. Mineral abbreviations: Bt–biotite, Ms–muscovite, Pl–plagioclase, Kfs–K-feldspar.

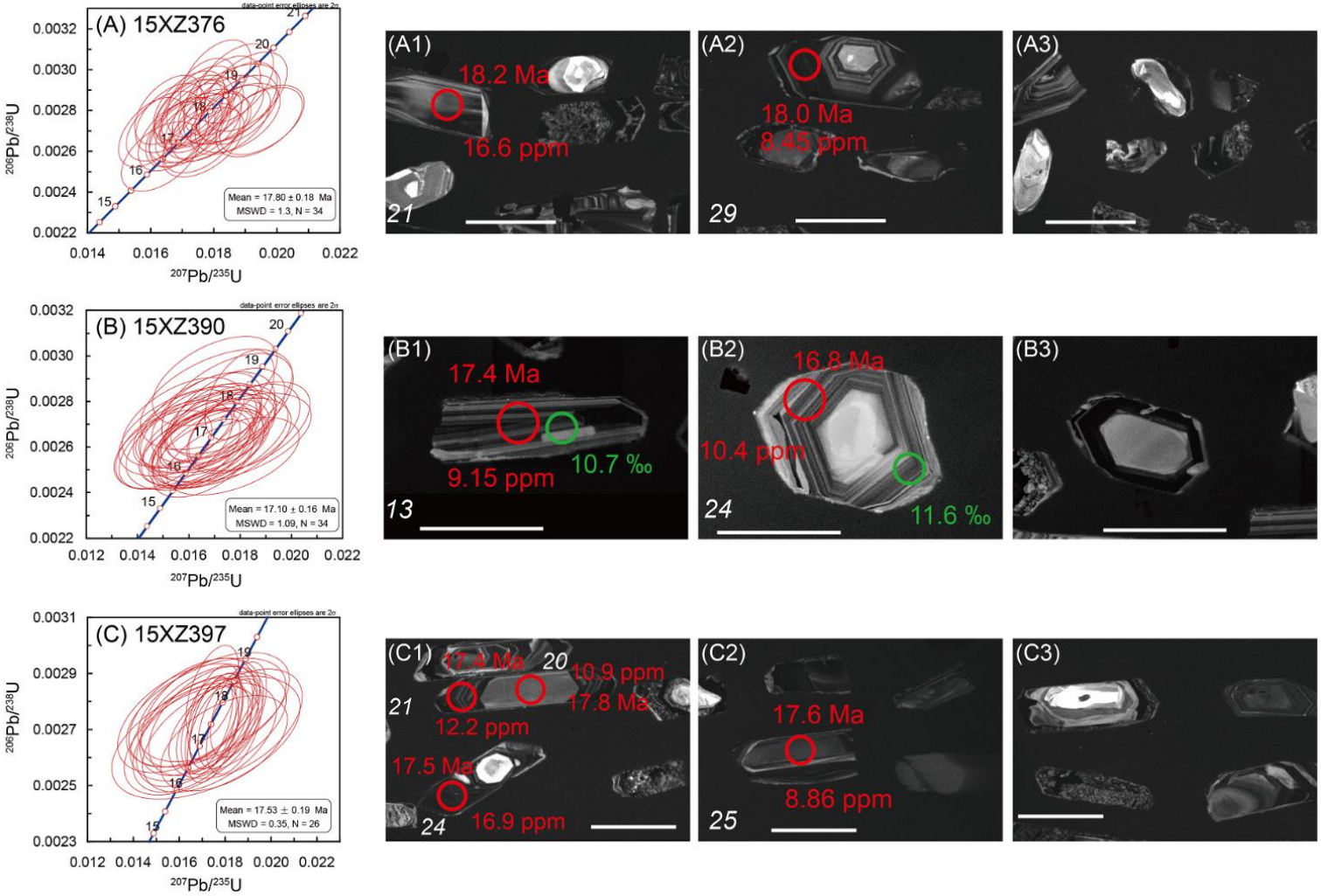

Figure S2. Zircon U–Pb concordia diagrams for the Yalaxiangbo granites (the first left panels; Table S1) and CL images of representative zircons from the Yalaxiangbo granites (the three right panels). Each row comes from the same sample. The green and red circles are analytical positions of O isotope and U–Pb isotopes + trace elements, with diagrams of 20 μm and 32 μm, respectively. Scale bar is 100 μm. Analytical results of U–Pb ages, $\delta^{18}O$ values and Ti contents are also labeled. The rightmost three images show relict zircon surrounded by dark and thin rims which cannot be analyzed. Analytical number is shown in white italic.

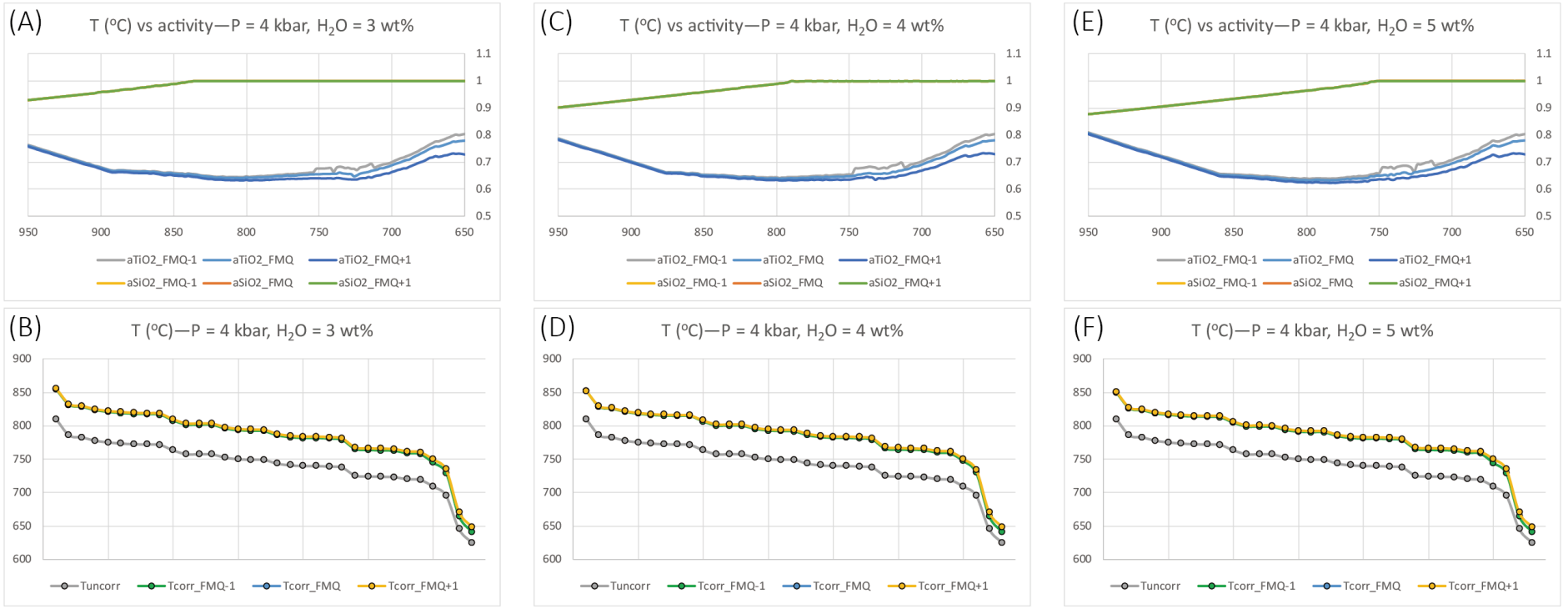

Figure S3. Results of condition experiments showing the influences of initial water content and oxygen fugacity on the activities (a_{SiO2} and a_{TiO2}) and corrected temperatures derived from Ti-in-zircon thermometer. Sample 15XZ390 is used for modeling. Crystallization pressure is set to 4 kbar. The modeling results are listed in Tables S3 and S4.

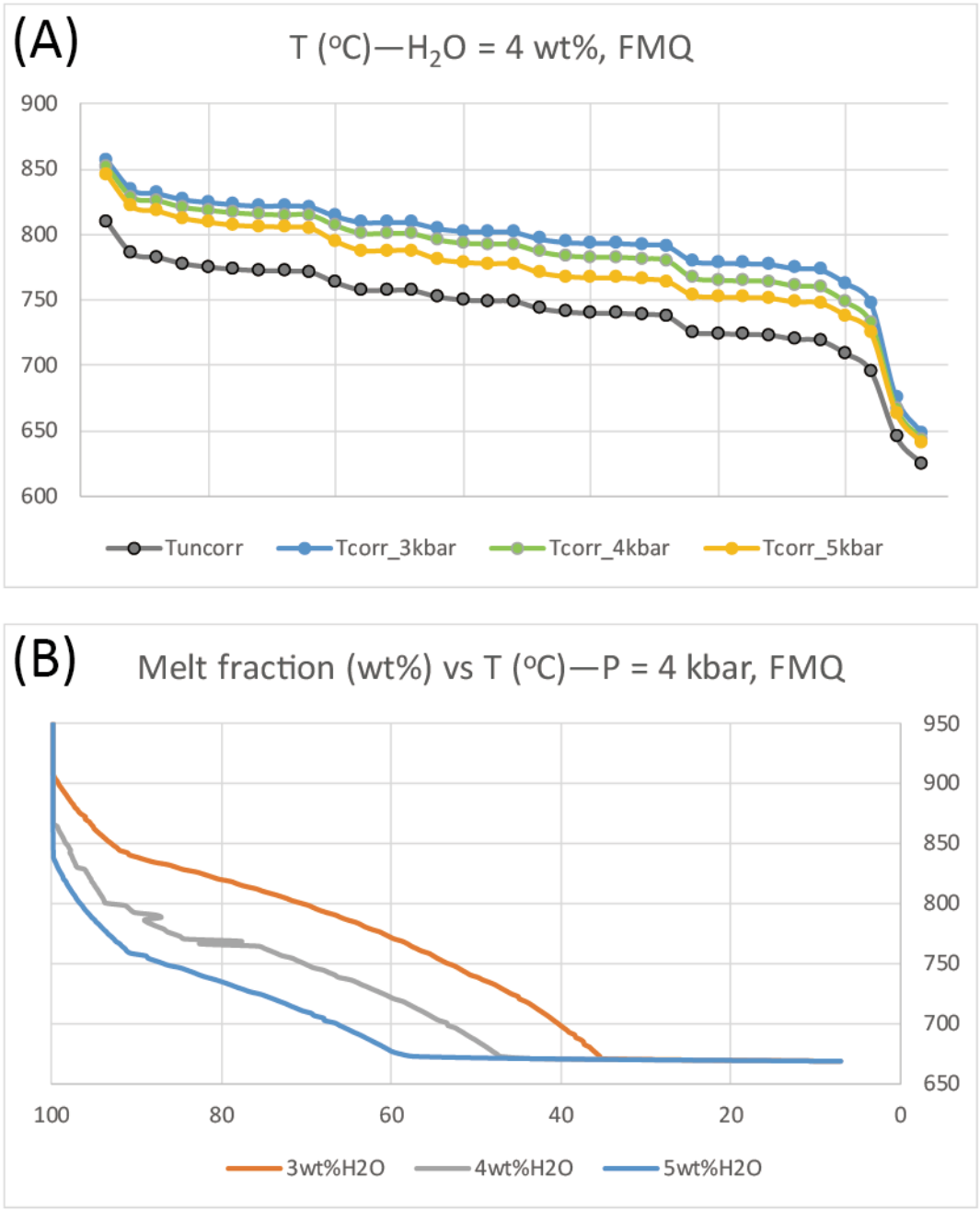

Figure S4. (A) Results of condition experiments showing the influence of crystallization pressure on the corrected temperatures derived from Ti-in-zircon thermometer. Sample 15XZ390 is used for modeling. Initial water content and oxygen buffer are set to 4 wt% and FMQ, respectively. The modeling results are listed in Table S3. (B) Results of modeled melt fraction (wt%) versus crystallization temperature. Crystallization pressure and oxygen buffer are set to 4 kbar and FMQ, respectively. Three initial water contents (3, 4, 5 wt%) are considered. The modeling results are listed in Table S4.

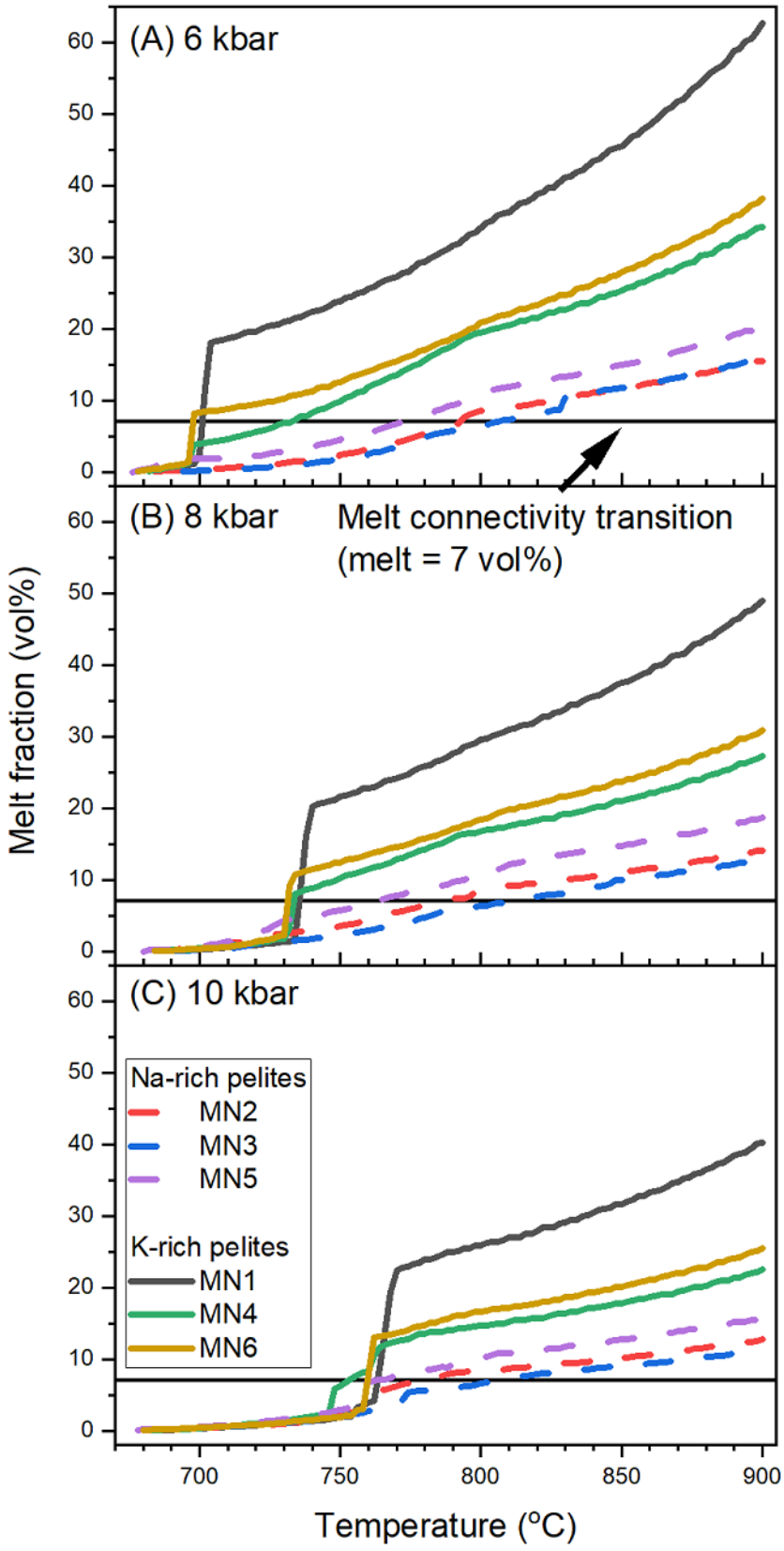

Figure S5. Results of modeled melt fraction (vol%) versus melting temperature derived from six pelite samples at 6, 8, and 10 kbar. Starting materials used for modeling are given is Table S5 and the modeling results are listed in Table S6. Oxygen buffer FMQ is used. 'Melt connectivity transition' from Rosenberg and Handy (2005) at 7 vol% melt is shown for comparison.

Rosenberg, C.L., and Handy, M.R., 2005, Experimental deformation of partially melted granite revisited: implications for the continental crust: Journal of Metamorphic Geology, v. 23, p. 19–28, https://doi.org/10.1111/j.1525-1314.2005.00555.x.

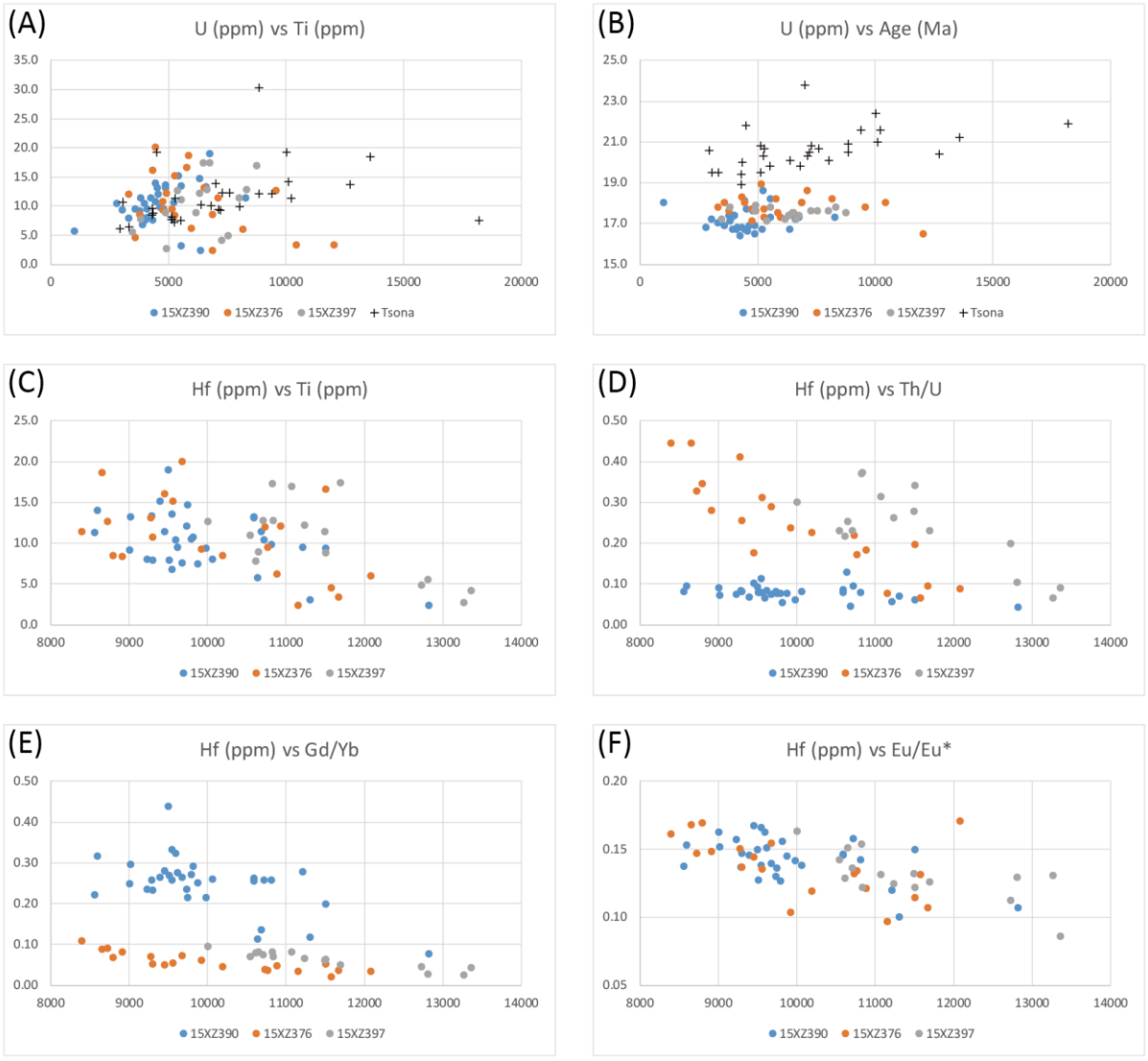

Figure S6. Plots of zircon trace element compositions of the three Miocene Yalaxiangbo granites. Data are given in Table S1. Data for Tsona granites in panels (A) and (B) are from Aikman et al. (2012b).

Aikman, A.B., Harrison, T.M., and Hermann, J., 2012b, Age and thermal history of Eo- and Neo-Himalayan granitoids, eastern Himalaya: Journal of Asian Earth Sciences, v. 51, p. 85–97, https://doi.org/10.1016/j.jseaes.2012.01.011.

Supplementary Materials II: Methodology

1. Whole-rock major-trace element analyses

Whole-rock major and trace elements were analyzed at the ALS Chemex (Guangzhou, China) Co., Ltd. Major element oxides were determined using an X-ray fluorescence spectrometer (XRF). All iron is given in the form of Fe_2O_3 in this determination. Analytical precision of major element oxides is better than ±2–5%. Trace elements were determined using PerkinElmer ICP-MS with the analytical precision better than ±5% for most elements. Whole-rock major-trace element analyses are listed in Table S2.

2. Whole-rock Sr–Nd isotope analyses

Whole-rock Rb–Sr and Sm–Nd isotope analyses were carried out on a mass spectrometer Finnigan TRITON at Tianjin Institute of Geology and Mineral Resources in Chinese Ministry of Land and Resources, Tianjin. Before the isotopic analyses, separation and purification were conducted at CAS Laboratory of Crust-Mantle Materials and Environments in University of Science and Technology of China (USTC), Hefei. About 100 mg whole-rock powders were dissolved in HF+HClO4 in Teflon capsules at 120°C for 7 days. After that, the solutions were dried and then dissolved in HCl for the separation of trace elements. Sr and LREE were separated with a second cation exchange column packed with AG50Wx12. Nd was separated from other rare earth elements using 1.7-ml Teflon powder coated with HDEHP, di(2-ethylhexyl)orthophosphoric acid, as cation exchange medium. The measured $^{87}Sr/^{86}Sr$ ratio of standard NBS987 and $^{143}Nd/^{144}Nd$ ratio of standard LRIG were 0.710240±0.000007 and 0.512198±0.000004, respectively. Whole-rock Sr–Nd isotope data are provided in Table S2.

3. LA-ICPMS zircon U–Pb isotope and trace element analyses

Zircon grains were extracted, mounted and polished to expose the grain centre for microbeam analyses. Cathodoluminescence (CL) and backscattered electron (BSE) images are taken for inspecting internal structures of individual zircons and selecting positions for U–Pb–O isotope and trace element in-situ analyses. Both optical and electron microscopy (CL and BSE) were used to examine zircon grains for cracks, inclusions and other imperfections which were avoided during analysis. Three samples (15XZ376, 15XZ390 and 15XZ397) were selected for U–Pb isotope and trace element analyses, while only sample 15XZ390 was analyzed for O isotopes. O isotope analysis was performed at first, then U–Pb isotopes, and trace elements at last. Analyses were carried out at adjacent positions or the same growth domains (Fig. S2).

Zircon U–Pb isotope analyses were carried out using LA-ICP-MS (Laser Ablation-Inductively Coupled Plasma-Mass Spectrometry) at CAS Laboratory of Crust-Mantle Materials and Environments in USTC, Hefei. A pulsed 193 nm ArF Excimer (GeoLas HD) with laser power of 6 mJ/cm^2 pulse energy at a repetition ratio of 4 Hz coupled to an Agilent 7900 quadrupole ICP-MS was used for ablation. Helium was used as carrier gas to provide efficient aerosol transport to the ICP and minimize aerosol deposition. The diameter of the laser ablation crater was 32 μm. Zircon 91500 was used as an external standard to normalize isotopic fractionation during isotope analysis. NIST610 glass was used as an external standard to normalize U, Th and Pb concentrations of the unknowns. Meanwhile, zircon standard GJ-1 was used for monitoring of the data quality. The detailed analytical procedure can be found in Liu et al. (2010). Mean ages for pooled U/Pb analyses are quoted with 95% confidence interval. Ninety analyses of GJ-1 yield a mean $^{206}Pb/^{238}U$ age of 606.7 ± 3.5 Ma (MSWD=0.17, 2σ), consistent within errors with the ID-TIMS result of 608.5 ± 0.4 Ma (2σ) (Jackson et al., 2004). Zircon U–Pb isotope data are listed in Table S1.

Off-line selection and integration of background and analyte signals, time-drift correction and quantitative calibration for U–Th–Pb dating were performed by ICPMSDataCal (Liu et al., 2010), and the common Pb correction was carried out using the EXCEL program of ComPbCorr#151 (Andersen, 2002).

Trace element compositions of zircon were determined by LA-ICP-MS employing an Element XR HR (High Resolution)-ICP-MS instrument (Thermo Fisher Scientific, Bremen, Germany) coupled to a 193nm ArF excimer laser system (Geolas HD, Lambda Physik, Göttingen, Germany) at the State Key Laboratory of Lithospheric Evolution, Institute of Geology and Geophysics, Chinese Academy of Sciences. The approach is similar to that outlined in Wu et al. (2018) with isotopes measured using a peak-hopping mode with a laser beam diameter of 32 μm and 5 Hz repetition rate. The laser energy density is ~4.0 J/cm^2. The Element XR is equipped with the so-called "jet-interface", comprising of a jet sample cone, an X-version skimmer cone and a high capacity vacuum pump (OnTool Booster 150, Asslar, Germany). This leads to signal enhancement in laser sampling mode by a factor of 3–5, resulting in an improved detection capability. Helium was employed as the ablation gas to improve the transporting efficiency of ablated aerosols. NIST SRM 612 reference glass

was used as calibration material and it recommended values are collected from Pearce et al. (1997). GJ-1 and 91500 zircon reference materials were analyzed for data quality control. Silicon (^{29}Si) was used as an internal standard. The resulting data were reduced based on the GLITTER program (Griffin et al., 2008). For most trace elements (>0.005 ppm), the accuracy is in a discrepancy of ±10 % with the analytical precision (1 RSD) of ±10%. Forty-six analyses of 91500 yield an average Ti content of 5.09±0.41 ppm (1SD), in agreement within error with the value of 4.73±0.15 ppm measured by ID (Isotope Dilution)-ICPMS (Szymanowski et al., 2018). Zircon trace element contents are presented in Table S1.

4. SIMS in-situ zircon O isotope analysis

Before U–Pb isotope analyses, zircon in-situ O isotopes were analyzed using Cameca IMS 1280-HR at State Key Laboratory of Isotope Geochemistry in Guangzhou Institute of Geochemistry, CAS, Guangzhou. Analytical procedures are the same as those described by Li et al. (2010a). The Cs^+ primary ion beam was accelerated at 10 kV, with an intensity of ca. 2 nA (Gaussian mode with a primary beam aperture of 200 μm to reduce aberrations) and rastered over a 10 μm area. The analysis spot was about 20 μm in diameter (10 μm beam diameter + 10 μm raster). Oxygen isotopes were measured in multi-collector mode using two off-axis Faraday cups. The NMR (Nuclear Magnetic Resonance) probe was used for magnetic field control with stability better than 2.5 ppm over 16 h on mass 17. One analysis takes ~3.5 min consisting of pre-sputtering (~30 s), 120 s of automatic tuning of the secondary beam, and 64 s of analysis. The instrumental mass fractionation (IMF) was corrected using in-house zircon standard Penglai with a recommended $\delta^{18}O$ value of 5.31±0.10‰ with reference to the Vienna standard mean oceanic water (VSMOW) that has a recommended $^{18}O/^{16}O$ ratio of 0.0020052 (Li et al., 2010b). The measured $^{18}O/^{16}O$ ratios for samples (raw data) were firstly normalized relative to the VSMOW, and then corrected for IMF (Li et al., 2010a).

The internal precision of a single analysis was generally better than ±0.20‰ (2σ standard error) for $\delta^{18}O$ values. The external precision, measured by the reproducibility of repeated analyses of the Penglai standard during two sessions of this study, is ±0.24‰ (2SD, n=14) and ±0.34‰ (2SD, n = 27). During the two sessions, a second zircon standard Qinghu was measured as an unknown to ascertain the veracity of the IMF. Two series of analyses in seven and twelve measurements of Qinghu zircon standard yield a weighted mean of $\delta^{18}O$ = 5.43 ± 0.14‰ (2SD) and 5.44 ± 0.12‰ (2SD). These values are in good agreement within errors with a reported value of 5.4 ± 0.2‰ (Li et al., 2013). Zircon O isotope data are listed in Table S1.

5. Laser O isotope analyses

Whole-rock O isotope analysis was performed by the laser fluorination technique using a Finnigan Delta XP mass spectrometer equipped with a 25 W MIR-10 CO2 laser at CAS Key Laboratory of Crust-Mantle Materials and Environments in USTC, Hefei. Repeat measurements gave analytical errors better than ±0.1‰ (1σ). Two reference minerals were used: $\delta^{18}O$ = 5.8‰ for garnet UWG-2 (Valley et al., 1995), and $\delta^{18}O$ = 10.0‰ for zircon 91500 (Zheng et al., 2004). Whole-rock O isotope data are listed in Table S2.

6. Mineral major element analysis

Fresh micas and plagioclase in polished thin sections from sample 15XZ390 were prepared for electron probe microanalyses. Elemental analyses were obtained using a JEOL JXA-8230 electron microprobe at Hefei University of Technology, China, under the conditions of 15 kV accelerating voltage, a beam current of 20 nA and a beam size of 5 μm. Standards used were natural minerals, including biotite (Mg, K, Fe, Ti), tremolite (Si), kyanite (Al), jadeite (Na), garnet (Ca, Mn), spinel (Cr) and apatite (F, Cl). ZAF correction method was used. Routine detection limits were 0.02 wt% for F and Cl, and 0.01 wt% for all other elements. Mineral major element data are listed in Table S8.

7. Phase equilibrium modeling

In this study, phase equilibrium modeling of magma crystallization and rock melting was performed in the MnNCKFMASHTO chemical system using the thermodynamic program Rcrust (Mayne et al., 2016), updated to version 2019.03.01, with a compiled form of the meemum function from the Perple_X suite of programs (Connolly, 2009). The thermodynamic dataset of Holland and Powell (2011) and the following activity-composition models were employed: biotite [Bi(W)], cordierite [Crd(W)], garnet [Gt(W)], melt [melt(W)], white-mica [Mica(W)], orthopyroxene [Opx(W)], and staurolite [St(W)] (White et al., 2014), clinopyroxene [Cpx(HP)] (Holland and Powell, 1996), epidote [Ep(HP11)] (Holland and Powell, 2011), ternary feldspar [Fsp(C1)] (Holland and Powell, 2003), ilmenite [Ilm(WPH)] (White et al., 2000), and spinel [Sp(WPC)] (White et al., 2002). Aluminosilicates, quartz, rutile and water were treated as pure phases.

7.1 T–a_{SiO2}–a_{TiO2} relation of magma crystallization

The activity of a chemical component in a thermodynamically closed system can be calculated by Equation 1 where the activity (a) of the chemical component (A) is a function of the chemical potential of the component at the pressure and temperature of interest ($\mu_A^{P,T}$) and the chemical potential of the pure substance at the pressure and temperature of interest ($\mu 0_A^{P,T}$) since G = μ for a pure substance.

$$a_A = e^{\left(\frac{\mu_A^{P,T} - \mu 0_A^{P,T}}{R \times T}\right)} \qquad \text{(Equation 1)}$$

Where:
a_A = activity of chemical component A (J/mol)
$\mu_A^{P,T}$ = chemical potential of chemical component A at pressure P and temperature T (J/mol)
$\mu 0_A^{P,T}$ = chemical potential of pure substance of A at pressure P and temperature T (J/mol)
R = molar gas constant = 8.3144598 $m^2kg.s^{-2}K^{-1}mol^{-1}$
T = Temperature (K)
e = eulers number = 2.71828

In order to acquire activities for SiO_2 and TiO_2 across a range of P–T space this calculation was automated in the phase equilibria modelling tool Rcrust (Mayne et al., 2016, 2019). Here chemical potentials are extracted from meemum from Perple_X (Connolly, 2009) first for the pure substance of interest (by setting the chemical system to only consist of this component) and then for the full system considered. In this way the activity of TiO_2 and SiO_2 for are calculated as

$$a_{TiO2} = e^{\left(\frac{\mu_{TiO2}^{P,T} - \mu 0_{Rutile}^{P,T}}{R \times T}\right)} \qquad a_{SiO2} = e^{\left(\frac{\mu_{SiO2}^{P,T} - \mu 0_{Quartz}^{P,T}}{R \times T}\right)}$$

Through the approach given above, the relation of T–a_{SiO2}–a_{TiO2} for a cooling magma system can be obtained. Here three granite samples which have been selected for zircon Ti analysis were used for modeling of magma crystallization (15XZ376, 15XZ390 and 15XZ397). Their whole-rock major element compositions (after anhydrous 100% correction) were taken as the compositions of starting materials. The following crystallization conditions were considered: pressure of 3, 4 and 5 kbar, initial water content of 3, 4 and 5 wt% and oxygen buffer of FMQ-1, FMQ and FMQ+1. Temperature ranges from 950 °C and 650 °C, with an interval of 2 °C. The obtained T–a_{SiO2}–a_{TiO2} relations for sample 15XZ390 at a variety of conditions were presented in Table S4 in Supplementary Materials III.

Combining the relation of T–a_{SiO2}–a_{TiO2} and the measured Ti content in zircon from granite samples, we can calculate the activity corrected Ti-in-zircon temperature using the equation calibrated by Ferry and Watson (2007), which is:

$$T\ (°C) = \frac{4800}{5.711 - \log(Ti\ in\ ppm) - \log(a_{SiO2}) + \log(a_{TiO2})} - 273.15 \quad \text{(Equation 2)}$$

During calculation, an initial temperature value (T_i) was assumed for each Ti content of zircon. Then, the corresponding values of a_{SiO2} and a_{TiO2} at the assumed temperature can be read according to the T–a_{SiO2}–a_{TiO2} relation. So a temperature value (T_f) was yielded according to equation 2. The value of T_i was then replaced by that of T_f. These steps were repeated until the difference between T_f and T_i is ≤ 2 °C. The final value of T_f is taken as the corrected Ti-in-zircon temperature. The uncorrected temperature was calculated from equation 2 with $a_{SiO2} = a_{TiO2} = 1$. The calculated results are listed in Table S3.

7.2. Partial melting of pelites

Six pelite samples from Aikman et al. (2012a) were used as the starting materials for modeling. Their major-element chemical compositions after anhydrous 100wt% correction are given in Table S5. Melting pressures and temperatures range from 6 kbar to 10 kbar with an interval of 2 kbar, and from 640 °C to 900 °C with an interval of 2 °C, respectively. To simulate a water-absent melting regime, the bulk composition of the system is set to start with an excess of water and phase extraction routines set such that free water is extracted whenever it is present, this process is described in detail in Mayne et al. (2019). Modeling was carried out at oxygen buffer of FMQ. The yielded results were reported in Tables S6 and S7.

References

Aikman, A.B., Harrison, T.M., Hermann, J., 2012a. The origin of Eo- and Neo-himalayan granitoids, Eastern Tibet. Journal of Asian Earth Sciences 58, 143–157.

Anderson, T., 2002. Correction of common lead in U−Pb analyses. Chemical Geology 192, 59–79.

Connolly, J.A.D., 2009. The geodynamic equation of state: what and how. Geochemistry, Geophysics,

Geosystems 10.
Ferry, J.M., Watson, E.B., 2007. New thermodynamic models and revised calibrations for the Ti-in-zircon and Zr-in-rutile thermometers. Contributions to Mineralogy and Petrology 154, 429–437.
Griffin, W. L., Powell, W.J., Pearson, N.J., O'Reilly, S.Y., 2008. GLITTER: data reduction software for laser ablation ICP-MS. Laser Ablation ICP-MS in the Earth Sciences: Current practices and outstanding issues 40, 308–311
Holland, T.J.B., Powell, R., 1996. Thermodymanics of Order-Disorder in Minerals. II. Symmetric Formulism Applied to Solid Solutions. American Mineralogist 81, 1425–1437
Holland, T.J.B., and Powell, R., 2003. Activity-composition relations for phases in petrological calculations: an asymmetric multicomponent formulation. Contributions to Mineralogy and Petrology 145, 492–501.
Holland, T.J.B., Powell, R., 2011. An improved and extended internally consistent thermodynamic dataset for phases of petrological interest, involving a new equation of state for solids. Journal of Metamorphic Geology 29, 333–383.
Jackson, S.E., Pearson, N.J., Griffin, W.L., and Belousova, E.A., 2004. The application of laser ablation-inductively coupled plasma-mass spectrometry to in situ U-Pb zircon geochronology. Chemical Geology 211, 47–69.
Li, X.H., Li, W.X., Li, Q.L., Wang, X.C., Liu, Y., Yang, Y.H., 2010a. Petrogenesis and tectonic significance of the 860 Ma Gangbian alkaline complex in South China: evidence from in situ zircon U-Pb dating, Hf-O isotopes and whole-rock geochemistry. Lithos 114, 1–15.
Li, X.H., Long, W.G., Li, Q.L., Liu, Y., Zheng, Y.F., Yang, Y.H., Chamberlain, K.R., Wan, D.F., Guo, C.H., Wang, X.C., Tao, H., 2010b. Penglai zircon megacrysts: a potential new working reference material for microbeam determination of Hf-O isotopes and U-Pb age. Geostandards and Geoanalytical Research 34, 117–134.
Li, X.H., Tang, G.Q., Gong, B., Yang, Y.H., Hou, K.J., Hu, Z.C., Li, Q.L., Liu, Y., Li, W.X., 2013. Qinghu zircon: a working reference for microbeam analysis of U-Pb age and Hf and O isotopes. Chinese Science Bulletin 58, 4647–4654.
Liu, Y.S., Gao, S., Hu, Z.C., Gao, C.G., Zong, K.Q., and Wang, D.B., 2010. Continental and oceanic crust recycling-induced melt–peridotite interactions in the trans-north China Orogen: U–Pb dating, Hf isotopes and trace elements in zircons from mantle xenoliths. Journal of Petrology 51, 537–571.
Mayne, M.J., Moyen, J.-F., Stevens, G., Kaislaniemi, L., 2016. Rcrust: a tool for calculating path-dependent open system processes and application to melt loss. Journal of Metamorphic Geology 34, 663–682.
Mayne, M., Stevens, G., Moyen, J.-F., Johnson, T., 2019. Performing process-oriented investigations involving mass transfer using Rcrust: a new phase equilibrium modelling tool. Geological Society, London, Special Publications SP491–2018–85.
Szymanowski, D., Fehr, M.A., Guillong, M., Coble, M.A., Wotzlaw, J.F., Nasdala, L., Ellis, B.S., Bachmann, O., Schönbächler, M., 2018. Isotope-dilution anchoring of zircon reference materials for accurate Ti-in-zircon thermometry. Chemical Geology 481, 146–154.
Valley, J.W., Kitchen, N., Kohn, M.J., Niendorf, C.R., Spicuzza, M.J., 1995. UWG-2, a garnet standard for oxygen isotope ratio: strategies for high precision and accuracy with laser heating. Geochim. Cosmochim. Acta 59, 5223–5231.
White, R.W., Powell, R., Holland, T.J.B., Worley, B.A., 2000. The effect of TiO2 and Fe2O3 on metapelitic assemblages at greenschist and amphibolite facies conditions: mineral equilibria calculations in the system K_2O-FeO-MgO-Al_2O_3-SiO_2-H_2O-TiO_2-Fe_2O_3. Journal of Metamorphic Geology 18, 497–512.
White, R.W., Powell, R., and Clarke, G.L., 2002. The interpretation of reaction textures in Fe-rich metapelitic granulites of the Musgrave Block, central Australia: constraints from mineral equilibria calculations in the system K_2O-FeO-MgO-Al_2O_3-SiO_2-H_2O-TiO_2-Fe_2O_3. Journal of Metamorphic Geology 20, 41–55.
White, R.W., Powell, R., Holland, T.J.B., Johnson, T.E., Green, E.C.R., 2014. New mineral activity-composition relations for thermodynamic calculations in metapelitic systems. Journal of Metamorphic Geology 32, 261–286.
Wu, S.T., Karius, V., Schmidt, B.C., Simon, K., Wörner, G., 2018. Comparison of Ultrafine Powder Pellet and Flux-free Fusion Glass for Bulk Analysis of Granitoids by Laser Ablation-Inductively Coupled Plasma-Mass Spectrometry, Geostandards and Geoanalytical Research 42, 575–591.
Zheng, Y.-F., Wu, Y.-B., Chen, F.-K., Gong, B., Li, L., Zhao, Z.-F., 2004. Zircon U–Pb and oxygen isotope evidence for a large-scale 18O depletion event in igneous rocks during the Neoproterozoic. Geochim. Cosmochim. Acta 68, 4145–4165.